WARSAW UNIVERSITY OF TECHNOLOGY Index 351733
FACULTY OF CIVIL ENGINEERING
COMMITTEE FOR CIVIL AND WATER ENGINEERING
POLISH ACADEMY OF SCIENCES ISSN 1230-2945

DOI: 10.24425/ace.2022.141899

ARCHIVES OF CIVIL ENGINEERING

Vol. LXVIII ISSUE 3 2022

pp. 501 –522

Research paper

Study on stability of self-compacting concrete applied for filling layer structure from paste, mortar and concrete

He Liu[1], Jingyi Zhang[2], Yanhai Yang[3]

Abstract: Self compacting concrete (SCC) filling layer is core structure of China rail track system (CRTS) ? type ballastless track. Construction quality, service performance and durability of CRTS ? ballastless structure are affected by stability of SCC for filling layer. In this study, the stability of SCC of filling layer is researched at three levels as paste, mortar and concrete by theory and experiment. Evaluation indices including bleeding (B), surface bubble rate (θ), thickness of paste (σ_{paste}) and thickness of surface mortar (L) are proposed based on the theoretical calculation and analysis. The threshold viscosity of paste 0.394 Pa·s and mixture satisfied area are obtained at paste level based on the relationship between viscosity and B, θ of paste. The mixture satisfied area was defined at mortar level under criterions of maximum value of σ_{paste} and slump flow. Optimal range of gap between neighboring aggregates (λ_{ca}) 12.4 mm~14.1 mm is chosen by flow ability, passing ability, stable ability of SCC. These research results will help to further understand the stability of SCC.

Keywords: stability, self-compacting concrete, filling layer, plastic viscosity, mix proportion

[1]PhD., Eng., Shenyang Jianzhu University, School of Transportation and Geomatics Engineering, No. 25 Hunnan Zhong Road, Hunnan District, 110168 Shenyang, China, e-mail: heliu@sjzu.edu.cn, ORCID: 0000-0002-3867-0726

[2]M. Eng., Shenyang Urban Construction University, School of Civil engineering, No.380 Bai Ta Road, Hunnan District, 110167 Shenyang, China, e-mail: dq_zjy@syucu.edu.cn, ORCID: 0000-0003-4641-5191

[3]Prof. PhD., Eng., Shenyang Jianzhu University, School of Transportation and Geomatics Engineering, No. 25 Hunnan Zhong Road, Hunnan District, 110168 Shenyang, China, e-mail: yangyanhai168@126.com, ORCID: 0000-0002-1599-7873

1. Introduction

The China Rail Track System (CRTS) III slab ballastless track has been more and more used in newly-built track structure applied in Chinese high-speed railway. It is typically composed of four layers, from top to bottom including prefabricated track slab, self-compacting concrete (SCC) filling layer, geotextile sheet and concrete base plate [1–3]. Geotextile sheet is manufactured by synthetic fiber, its main function includes insulating SCC filling layer and concrete bottom; decreasing the stress amplitudes caused by temperature gradient stress and further avoiding fracture in SCC filling layer-concrete bottom interface. Furthermore, the geotextile sheet can be replaced with a damping layer when surrounding buildings require low ambient vibration and ambient noise. The damping layer is mainly composed of natural rubber, it has a similar effect as geotextile sheet and can also improve the energy absorption characteristics of CRTS III slab ballastless track [4], [5]. SCC filling layer as a key component, its main functions include ensuring the correct position of above prefabricated slab and transferring train-load. SCC filling layer is a panel layer with upper track slab and concrete base plate. Compared with the traditional application conditions of SCC, normal SCC is often cast into an open formwork. The top surface of SCC can be smoothed by the process of finishing, so slight bleeding and rising of bubbles are acceptable. However, SCC applied in the slab track is grouted into a flat, narrow and sealed space with an area of about 14 m^2 and a thickness of 90 mm. At the same time, according to the design theory, it is required that excellent bonding strength between filling layer and track plate. Thus, bleeding, surface settlement and instability of bubbles should be strictly controlled. Furthermore, the filling layer structure is complex, such as steel mesh, gate steel bar, limited groove and geotextile layers. Comprehensive consideration of structural characteristics and design requirements, SCC for filling layer should have good fluidity, passing ability, especially the stability of SCC should be proper design.

According to engineering practice, SCC with excellent flow ability and passing ability will fill whole board cavity smoothly. But the interface region between track slab and filling layer will be formed when stability of SCC is poor. The interface region includes water and bubble layer, paste layer and mortar layer. The interface region will lead to form initial defects, such as laitance layer, bubble, water wave, foaming laye. Durability, safety and service performance of slab ballastless track structure are affected by the initial defects. Therefore, excellent stability is necessary of SCC for filling layer.

Many researchers paid attention to stability of SCC and got many interesting results. Research results including two aspects: one aspect is stability testing methods of SCC; another aspect is that SCC stability is influenced by mix proportion and rheological parameter. Testing methods of stability of SCC mainly include rapid testing method [6], modified Segregation Prob [7], Plastic settlement strain device [8, 9], column segregation test [10, 11], electrical conductivity method [12], tilting box [13], flow-through test [14], slump flow [15], V-funnel, L-box, U-box, J-ring tests [16, 17], etc. Static segregation can be predicted by first five test method, other test methods mainly focus on dynamic stability of SCC. There are many mix proportion parameters and rheological parameters, such as ag-

gregate properties, water to binder ratio, mineral admixtures, superplasticizer, yield stress and plastic viscosity. Aggregate applied in SCC, which play an important role in stability of SCC. Research result reported that SCC is easy more to prone to segregation with increasing of aggregate density and maximum particle size [18,19]. Koura et al. [20] reported that optimizing well-graded particle and paste volume was an effective method for enhancing the stability of SCC. The water to binder ratio is dominant method of controlling the fluidity of SCC and have important impacts on its stability. SCC stability is reduced with increasing the water to binder ratio [21,22]. Esmaeilkhanian et al. [18] found that reduction in water to binder ratio from 0.4~0.33 improved stability significantly, but further decreasing in water to binder ratio did not affect the stability. Many types of mineral admixtures, such as fly ash, metakaolin, limestone powder and silica fume have different influence on the stability of SCC. Silica fume and metakaolin had more significant effect on the stability of SCC due to its high fineness [23]. Amini et al. [24] found that segregation index of SCC blend of fly ash was increased due to spherical particle and smooth surface of fly ash. Ghoddousi et al. [25] concluded that partial replacement of cement by limestone powder decreased the stability of SCC, which was related to its low specific area. Generally, higher dosage superplasticizer increased the segregation tendency of SCC, furthermore it is noticeable in case of dynamic [22]. Rheological parameters (yield stress and plastic viscosity) of cement paste of SCC is determined by mix proportion, which are considered to be closely related to the stability of SCC. SCC is low segregation tendency with increasing yield stress and plastic viscosity [19,26].

Filling layer of CRTS ? slab ballastless track is characterized as a flat, narrow and sealed structure, which is constructed by SCC. SCC applied as filling layer must have excellent flow ability, high segregation resistance, no bleeding, and no settlement. SCC applied for filling layer requires elaborate design and preparation in order to satisfy the corresponding property requirements. Therefore, the objectives of this study are to investigate stability of SCC from paste, mortar and concrete by theory and experiment. At paste level, pastes with different admixtures were prepared, and rheological properties were measured. The relationship between rheological parameter and paste stability was revealed. At mortar level, the stability of mortar was researched with different plastic viscosity pastes and layer thickness of pastes. At concrete level, a new index and its threshold was proposed. These research results can enhance the quality of SCC for filling layer.

2. Theoretical research

2.1. Stability of paste

The fresh paste is consisted of liquid phase, solid phase and gas phase. Liquid phase consists of water and water reducer. Solid phase consists of cement and mineral admixture particles. Gas phase is air. Schematic diagram of composition of fresh paste is shown in Fig. 1. There will be relative movement trend due to the density difference of these phases. Bubble and free water move upward. Cement and mineral admixture particles will move

downward. The velocity of motion satisfies Stockes formula, as shown in Eq. (2.1) [27]. From Eq. (2.1), it is shown that velocity is inversely proportional to the viscosity of the paste and is directly proportional to diameter and density difference of particle. The velocity of motion needs to be close to zero when phases of the paste are stable. The viscosity of paste should be carefully selected to ensure the stability of each phase. In this paper, the viscosity of the paste is controlled to ensure the stability of the paste. At the same time, bleeding (B) and bubble rate (θ) are used to evaluate stability of paste.

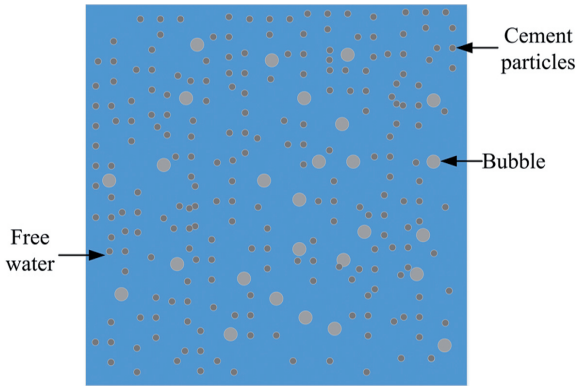

Fig. 1. Schematic diagram of composition of fresh paste

$$v_e = \frac{gr^2 \left|\Delta_\rho\right|}{18\eta} \tag{2.1}$$

where: v_e is Settling velocity of particles; r is Radius of particles or bubbles; η is plastic viscosity of paste; Δ_ρ is density difference; g is acceleration of gravity.

2.2. Stability of mortar

Segregation is unacceptable when SCC is flowing. SCC system can be regarded as composed of mortar and coarse aggregate. In slump flow test of SCC, segregation resistance criterion can be defined which should not exceed a threshold (the gap between neighboring aggregate) during the flowing time of SCC, as shown in Eq. (2.2) [28].

$$\int_0^{T_f} v_e d_t = \int_0^{T_f} \left(\frac{2\Delta_\rho g r^2}{9\eta_{\text{mortar}}}\right) d_t \leq \lambda_{\text{ca}} \Rightarrow \eta_{\text{mortar}} \geq \frac{2T_f \Delta_\rho g r^2}{9\lambda_{\text{ca}}} \tag{2.2}$$

where: T_f is time of slump flow and its value is 18s, λ_{ca} is Spacing of neighboring coarse aggregate, η_{mortar} is plastic viscosity value of mortar which can be calculated by Eq. (2.3) [29, 30].

$$\eta_{\text{mortar}} = \eta_{\text{paste}} \times \left(\frac{1 - V_S}{\phi_{\max}}\right)^{-[\eta]\phi_{\max}} \tag{2.3}$$

where: η_{paste} is viscosity of paste, $[\eta]$ is intrinsic viscosity, for non-circular particle systems, the value is about 4.5, V_s is volume fraction sand, $\phi_{\max}$ is maximum solid concentration which can be calculated by Eq. (2.4).

$$\phi_{\max} = \frac{\rho_{\text{packing}}}{\rho} \tag{2.4}$$

where: ρ is apparent density of sand; ρ_{packing} is packing density; it can be calculated by Eq (2.5) through A3-parameter packing density model 0.

$$\rho_{\text{packing}} = 1 \Bigg/ \left[\sum_{k=1}^{n} \frac{y_k}{\phi_k} - \sum_{j=1}^{i-1} (1 - b_{ij}) (1 - \phi_j) \frac{y_i}{\phi_j} \left[1 - c_{ij} \left(2.6^{\sum_{j=1}^{i-1} y_i} - 1 \right) \right] - \sum_{j=i+1}^{n} (1 - a_{ij}) \frac{y_j}{\phi_j} \left[1 - c_{ij} (3.8^{y_j} - 1) \right] \right] \tag{2.5}$$

where: y_i is the volumetric fraction of size class I; ϕ_i is the packing density of size class i; a_{ij}, b_{ij}, c_{ij} are the loosing effect parameter, wall effect parameter and wedging effect parameter respectively, they are calculated by Eq. (2.6), Eq. (2.7) and Eq. (2.8).

$$a_{ij} = 1 - (1 - s)^{7.1} - 1.9 \cdot s \cdot (1 - s)^{3.1} \tag{2.6}$$

$$b_{ij} = 1 - (1 - s)^{2.2} - 0.7 \cdot s \cdot (1 - s)^{9.3} - 0.2 \cdot (1 - s)^{10.6} \tag{2.7}$$

$$c_{ij} = 0.335 \cdot \tanh(26.9 \cdot s) \tag{2.8}$$

where s is characteristic size, it is calculated by Eq (2.9).

$$s = \sqrt{d_{\text{lower}} \times d_{\text{upper}}} \tag{2.9}$$

where d_{lower} is lower sieve size; d_{upper} is upper sieve size.

Combining Eq. (2.2) and Eq. (2.3), the minimum volume fraction of sand in the mortar can be obtained when SCC does not segregate during slump flow. It is presented in Eq. (2.10).

$$V_s \geq \phi_{\max} \left[1 - \left(\frac{9 \lambda_{\text{ca}} \eta_{\text{paste}}}{2 T_f \Delta_\rho g r^2} \right)^{\frac{1}{[\eta] \phi_{\max}}} \right] \tag{2.10}$$

The minimum volume fraction of sand is calculated by Eq. (2.10). But mortar is consisted of paste and sand. The paste must be enough to fill the voids between the sand and create a paste layer (σ_{paste}). Flow ability of mortar is excellent with thicker σ_{paste} but the stability of mortar is poor. Therefore, the flow ability and stability are influenced by σ_{paste}. The diagram of σ_{paste} is shown in Fig. 2 and it is calculated by Eq. (2.11).

$$\sigma_{\text{paste}} = \frac{V_p - V_s \times (1 - \phi_{\max})}{S} \tag{2.11}$$

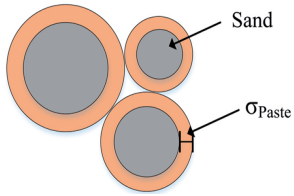

Fig. 2. Schematic diagram of thickness of paste layer

where: V_p is volume of paste; S is total surface area of sand, it is calculated by Eq. (2.12).

$$S = 4\pi \left(\frac{d_{\text{av}}}{2}\right)^2 \times N \tag{2.12}$$

where: d_{av} is average diameter of sand, according to Bui et al [32]. It is calculated by Eq. (2.13); N is number of equipment sand, it is calculated by Eq. (2.14).

$$d_{\text{av}} = \frac{\sum_i^n d_i m_i}{\sum_i^n m_i} \tag{2.13}$$

where: d_i is average diameter of class i (average size of two continuous sieve diameters); m_i is mass fraction of class i;

$$N = \frac{V_s}{\frac{4}{3}\pi \left(\frac{d_{\text{av}}}{2}\right)^3} \tag{2.14}$$

The threshold value of σ_{paste} is obtained when SCC is not segregation in the flow process under different viscosity of pastes. The threshold value of σ_{paste} is calculated by Eq. (2.15). The Eq. (2.15) can be obtained by combining Eq. (2.10) and Eq. (2.11).

$$\sigma_{\text{paste}} \leq \frac{V_p - \phi_{\max} \times (1 - \phi_{\max}) \left[1 - \left(\frac{9\lambda_{\text{ca}}\eta_{\text{paste}}}{2T_f \Delta_\rho g r^2}\right)^{\frac{1}{[\eta]\phi_{\max}}}\right]}{S} \tag{2.15}$$

2.3. Stability of concrete

SCC can be regarded as coarse aggregate particles suspended in the mortar. Systematic research was made on the spacing between the coarse aggregates in asphalt mixtures [33–35]. In cement paste, the schematic diagram is shown in Fig. 3. If the coarse aggregate is distributed in the mortar uniformly, the spacing between the coarse aggregates (λ_{ca}) is constant. Meanwhile, thickness of top surface mortar should be half of λ_{ca}. Workability of

SCC is influenced by the value of λ_{ca} when the property of mortar is constant. Flow ability and passing ability of SCC are poor when λ_{ca} is too closed. The flow ability and passing ability of SCC are enhanced when λ_{ca} is increasing. But the thickness of top surface mortar of SCC is increased with larger λ_{ca}. It will lead to the formation of a gradient structure between filling layer and track slab. Consequently, flow ability, passing ability and stability of SCC is influenced by λ_{ca} directly.

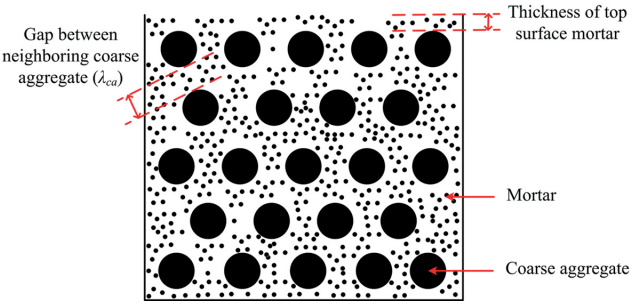

Fig. 3. Schematic diagram of SCC composition

In order to comprehend λ_{ca}, the concept of mean free path proposed by fullman and the stereology theory are employed to make some analysis in following sections, which can well deal with the particles distribution in three-dimensional system [36, 37]. As to the binary mixtures including the dispersed phase (particle or aggregate) and continuous phase (paste), λ_{ca} can be expressed by Eq. (2.16) according to fullman theory. Moreover, Eq. (2.17) can be established as followings according to the stereology theory.

$$\lambda_{ca} = \frac{[1 - V_a]}{N_L} \tag{2.16}$$

$$S_a = 2P_a, \qquad P_a = 2N_a \tag{2.17}$$

where: V_a is the volume fraction of particle in mixture. N_L is the number of particles a contacted the unit length line which passes the mixture. S_a is the specific area of particles a in unit volume mixture, 1/m. P_a is the number of unit length line contacted particles boundary when the line passes the system.

Thus, Eq. (2.18) can be obtained by combining the Eq. (2.16) and Eq. (2.17).

$$\lambda_{ca} = \frac{4[1 - V_a]}{S_a} \tag{2.18}$$

On the other hand, one can obtain the size distribution of particles (aggregate) by sieve test or fuller function. The amount of particles in different sizes satisfies the fuller function as following Eq. (2.19).

$$P_V(x) = \frac{\left(\sqrt{x} - \sqrt{D_{\min}}\right)}{\left(\sqrt{D_{\max}} - D_{\min}\right)} \tag{2.19}$$

where: $P_V(x)$ is the accumulative volume fraction of aggregate of size x, $D_{\max}$ and $D_{\min}$ are the maximum diameter and minimum diameter of aggregate, respectively.

The relationship between the total volume and specific area of aggregate in unit volume system can be expressed as Eq. (2.20). Then, Eq. (2.21) can be obtained by combining the Eq. (2.20) and Eq. (2.18).

$$S_a = \frac{6V_a}{\sqrt{D_{\max} \times D_{\min}}} \tag{2.20}$$

$$\lambda_{ca} = \frac{2(1 - V_a)}{3V_a} \times \sqrt{D_{\max} \times D_{\min}} \tag{2.21}$$

3. Experimental program

3.1. Materials and mixture proportions

3.1.1. Materials

The cementitious materials used in this experiment include P.O 42.5 cement (C), fly ash (FA), ground granulated blast slag (GGBS), hydroxypropyl methylcellulose (HPMC), silica fume (SF), limestone powder (LP), viscosity modified agent (VMA). The physical properties and chemical compositions of C, FA, GGBS, SF, LP are listed in Table 1. Solid content of superplasticizer (SP) is 30% and water-reducing rate of SP is 30%. Mixing water (W) is tap water. The VMA is composed of polymer, inorganic ultrafine calcareous and siliceous powder. The properties of VMA are listed in Table 2. Aggregate used in this study consists of sand (S) and coarse aggregate (G), gradation composition of sand and coarse aggregate are shown in Table 3.

Table 1. Physical properties and chemical composition of C, FA, GGBS, SF, LP, (by wt%)

Type	SiO_2	Al_2O_3	Fe_2O_3	CaO	MgO	SO_3	eq-Na_2O	Los on ignition	Specific surface area m^2/kg	Apparent density g/cm^3
C	24.6	7.30	4.00	59.7	3.8	2.5	0.60	2.50	350	3.12
FA	52.3	26.3	9.70	3.70	1.20	1.20	1.80	4.70	450	2.45
GGBS	26.1	13.8	14.1	33.6	8.10	–	0.45	2.10	420	2.87
SF	90.6	0.60	1.50	0.30	0.60	1.30	–	1.80	17800	2.1
LP	0.07	0.04	0.02	58.3	–	0.03	–	43.96	573	2.63

Table 2. Properties of VMA

Item	Chloride content (wt%)	Alkali content (wt%)	Viscosity ratio (%)	Bleeding (%)
Content	0.3	0.9	317	0

Table 3. Gradation composition of coarse aggregate and sand

Item		Size/mm								Fineness modulus
		16	9.5	4.75	2.36	1.18	0.6	0.3	0.15	
Coarse aggregate	Passing percentage/%	100	47.6	0.0	–	–	–	–	–	–
Sand-1		–	–	95.0	86.0	77.0	58.0	35.0	1.0	2.3
Sand-2		–	–	92.0	76.0	69.0	55.0	28.0	2.0	2.5
Sand-3		–	–	95.0	82.0	64.0	45.0	26.0	1.0	2.7
Sand-4		–	–	95.0	81.0	67.0	46.0	14.0	1.0	2.8
Sand-5		–	–	98.0	82.0	54.0	35.0	23.0	2.0	3.0

3.1.2. Mixing proportions

(1) Mixing proportions of paste

The mixing proportions of paste are listed in Table 4. Six series of paste were designed for rheological test, bleeding test, bubble stability test. The difference is the dosage of FA, GGBS, SF, LP, VMA and water to binder ratio. Several contents of FA (0%, 15%, 35%), GGBS (0%, 15%, 35%), SF (2%, 3%, 4%, 5%), LP (5%,10%,15%, 20%), VMA (2%, 3%, 4%, 5%, 6%, 7%) and water to binder ratio (0.32, 0.33, 0.34, 0.35, 0.36) were used to product paste. The mass ratio of SP dosage was fixed at 1.2%.

(2) Mix proportions of mortar

To study the roles of layer thickness of paste (σ_{paste}) in the fluidity and stability of mortar, an experimental program was launched, in which mortar mixes with different fineness modulus of sand (2.3, 2.5, 2.7, 2.8, 3.0), different sand to mortar ratios by volume (V_s/V_m, 0.4, 0.42, 0.44, 0.45, 0.46, 0.50) and different mix proportions of paste (P-16,

Table 4. Mixing proportions of paste

No.	C	FA	GGBS	HPMC	SF	LP	VMA	W/B	SP/%
P-1	100	0	0	0.03	0	0	0	0.34	1.2
P-2	65	35	0	0.03	0	0	0	0.34	1.2
P-3	65	0	35	0.03	0	0	0	0.34	1.2
P-4	65	15	20	0.03	0	0	0	0.34	1.2
P-5	63	15	20	0	2	0	0	0.34	1.2
P-6	62	15	20	0	3	0	0	0.34	1.2

Continued on next page

Table 4 [cont.]

No.	C	FA	GGBS	HPMC	SF	LP	VMA	W/B	SP/%
P-7	61	15	20	0	4	0	0	0.34	1.2
P-8	60	15	20	0	5	0	0	0.34	1.2
P-9	60	15	20	0	0	5	0	0.34	1.2
P-10	55	15	20	0	0	10	0	0.34	1.2
P-11	50	15	20	0	0	15	0	0.34	1.2
P-12	45	15	20	0	0	20	0	0.34	1.2
P-13	63	15	20	0	0	0	2	0.34	1.2
P-14	62	15	20	0	0	0	3	0.34	1.2
P-15	61	15	20	0	0	0	4	0.34	1.2
P-16	60	15	20	0	0	0	5	0.34	1.2
P-17	59	15	20	0	0	0	6	0.34	1.2
P-18	58	15	20	0	0	0	7	0.34	1.2
P-19	60	15	20	0	0	0	5	0.32	1.2
P-20	60	15	20	0	0	0	5	0.33	1.2
P-21	60	15	20	0	0	0	5	0.35	1.2
P-22	60	15	20	0	0	0	5	0.36	1.2
P-23	59	15	20	0	0	0	6	0.32	1.2
P-24	59	15	20	0	0	0	6	0.33	1.2
P-25	59	15	20	0	0	0	6	0.35	1.2
P-26	59	15	20	0	0	0	6	0.36	1.2
P-27	58	15	20	0	0	0	7	0.32	1.2
P-28	58	15	20	0	0	0	7	0.33	1.2
P-29	58	15	20	0	0	0	7	0.35	1.2
P-30	58	15	20	0	0	0	7	0.36	1.2

P-17, P-18 were listed in Table 4) were tested. Therefore, 90 mix proportions of mortar were prepared.

(3) Mix proportions of concrete

A total of 18 concrete mixes with varying η_{paste}, σ_{paste} and λ_{ca} were produced for workability test. Each concrete mix was assigned a mix number of $\eta_{\text{paste}} - \sigma_{\text{paste}} - \lambda_{\text{ca}}$, as listed in Table 5.

Table 5. Mix proportion of concrete

Mix No.	C	FA	GGBS	VMA	W	SP/%	S	G(5–10)	G(10–16)
0.394-0.191-16.5	342	86	114	29	194	1.2	855	281	421
0.394-0.193-14.9	334	84	111	28	189	1.2	827	302	454
0.394-0.195-13.6	326	81	109	27	185	1.2	799	324	486
0.394-0.197-12.4	317	79	106	26	180	1.2	771	346	518
0.394-0.200-11.3	309	77	103	26	175	1.2	743	367	551
0.394-0.202-10.3	300	75	100	25	170	1.2	716	389	583
0.484-0.191-16.5	337	86	114	34	194	1.2	855	281	421
0.484-0.193-14.9	328	84	111	33	189	1.2	827	302	454
0.484-0.195-13.6	320	81	109	33	185	1.2	799	324	486
0.484-0.197-12.4	312	79	106	32	180	1.2	771	346	518
0.484-0.200-11.3	304	77	103	31	175	1.2	743	367	551
0.484-0.202-10.3	295	75	100	30	170	1.2	716	389	583
0.616-0.191-16.5	331	86	114	40	194	1.2	855	281	421
0.616-0.193-14.9	323	84	111	39	189	1.2	827	302	454
0.616-0.195-13.6	315	81	109	38	185	1.2	799	324	486
0.616-0.197-12.4	307	79	106	37	180	1.2	771	346	518
0.616-0.200-11.3	299	77	103	36	175	1.2	743	367	551
0.616-0.202-10.3	290	75	100	35	170	1.2	716	389	583

3.2. Test methods

(1) Rheological test

Rheology was measured using "RheoPlus QC" coaxial cylinder rotary rheometer. The type of rotator was ST22-4V-40 and an outer tube of 163 ml volume with 42 mm diameter and 118 mm length. The temperature of samples was controlled at 25 ±1° by water bath. Rheological test of paste was tested at 5 minutes after mixing. The shearing rate was increased gradually from 1 S^{-1} to 200 S^{-1}, and then decreased from 200 S^{-1} to 1 S^{-1}. Yield stress and plastic viscosity of paste were obtained through fitting rheological curve by Eq (3.1).

$$\tau = \tau_0 + \eta\gamma + c\gamma^2 \tag{3.1}$$

where: τ is shear stress (Pa), τ_0 is yield stress (Pa), η is plastic viscosity (Pa·s), γ is shear rate (S^{-1}), C is constant.

(2) Bubble stability test

The equivalent mortar was prepared by CEM equivalent mortar method [38, 39]. The principle of equivalent mortar is that coarse aggregate in concrete was replaced by sand

with equal surface area. The bubble stability is performed using a novel test method [40], schematic diagram of test device is shown in Fig. 4. Firstly, the test device was placed horizontally, then the mortar was slowly and continuously injected into the device from the filling hole at the height of 100 mm, until the mortar stopped filling when the whole cavity was filled and mortar began to escape from exhaust vent. Secondly, after 24 hours, Photographs of surfaces of samples were taken using a single lens reflex camera. These photographs were imported into the image analysis software Image-Pro Plus. Diameter of bubbles were calculated by software. The number of bubbles with different diameters ($D > 5$ mm) and surface bubble rate θ can be obtained. Bubble rate θ was calculated by Eq (3.2).

$$\theta = \left[\pi\left(\sum\left(\frac{D_{0.5\sim1}}{2}\right)^2 + \sum\left(\frac{D_{1\sim2}}{2}\right)^2 + \sum\left(\frac{D_{3\sim4}}{2}\right)^2 + \sum\left(\frac{D_{4\sim5}}{2}\right)^2 + \sum\left(\frac{D_{\geq5}}{2}\right)^2\right)\right] \Big/ S \times 100\% \tag{3.2}$$

where: θ is surface bubble rate, S is the surface area of specimen, D is diameter of bubble.

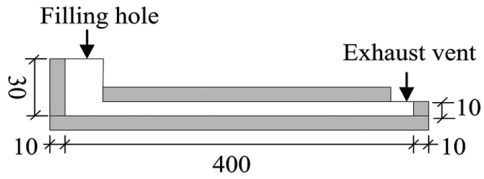

Fig. 4. Schematic diagram of the bubble stability test device

(3) Bleeding test

The bleeding of paste was tested according to Chinese National Standard JTG3420-2020 [39]. The testing procedure is as follow, after mixing, a 250 ml graduated cylinder made of glass was adopted to measure the bleeding rate of paste. The volume of paste ranges from 200~230 ml for all tests. After filling, graduated cylinders were sealed by plastic film. For each paste, bleeding water thicknesses were successively measured by reading the scale after 2 hours, testing picture is shown in Fig. 5. Then bleeding rate of

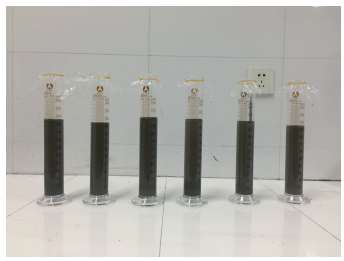

Fig. 5. Picture for bleeding test

paste was calculate by Eq. (3.3).

$$B = \frac{V_W}{V_{\text{paste}}} \times 100\% \tag{3.3}$$

where: B is bleeding of paste (%), V_w is volume of bleeding water (ml), V_{paste} is volume of paste (ml).

(4) Workability test

Slump flow of mortar was measured by spread cone as shown in Fig. 6. Slump flow, T500 and passing ability of SCC were determined by experiments according to ASTM C1611 [42] and C1621 [43]. Thickness of surface paste (L) was tested by a novel test method [2, 44].

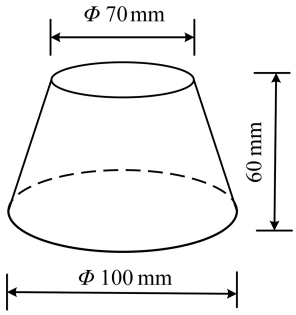

Fig. 6. Internal dimensions of spread cone

4. Results and discussion

4.1. Rheological property of paste

The test results of rheological parameters of fresh paste with different cementitious compositions, including yield stress and plastic viscosity are shown in Fig. 7. As illustrated in Fig. 7a, contract to cement paste, yield stress and plastic viscosity descend 4.6% and 41.1% for 35% FA by weight replacement, but yield stress and plastic viscosity increase 34.1% and 8.9% for 35% GGBS by weight replacement. On the other hand, yield stress descends 26.8% and plastic viscosity increase 100% for 15% FA and 20% GGBS by weight replacement. Rheological properties of paste are the essential workability characteristic of SCC, which is very important for fresh SCC. SCC can flow easily with low yield stress paste. High plastic viscosity of paste takes great influence on stability of SCC. According to the test result as shown in Fig. 7a, the rheological properties of paste with 15% FA and 20% GGBS by weight replacement meets the requirements of paste in SCC. Based on this research result, paste was prepared with 15% FA and 20% GGBS by weight replacement, while SF, LP and VMA were used to replace cement with 2~5%, 5~20% and 2~7% of total mass of cementitious material, respectively. Rheological test results of these mixes are

shown in Fig. 7b, Fig. 7c and Fig. 7d, respectively. From Fig. 7b and Fig. 7d, yield stress and plastic viscosity is gradually increasing with increasing SF and VMA replacement. SF having a large specific surface area and VMA consisting of cellulose and ultrafine inorganic powder are the main causes of the increasing yield stress and plastic viscosity of paste. From Fig. 7c, the yield stress and plastic viscosity of paste descend with LP content from 5~15%. The yield stress and plastic viscosity of paste increase with 20% LP content. The yield stress and plastic viscosity of paste descend with LP content from 5% to 15%. The main reason is that the void of the cementitious system is filled by LP particles, free water of cementitious system will be released. However, when the content of LP increases from 15% to 20%, the void of cementitious system is filled totally and the remaining LP particles needs more free water to wrap which reduces the content of free water of paste. Ultimately, it leads to that yield stress and plastic viscosity of paste are increased.

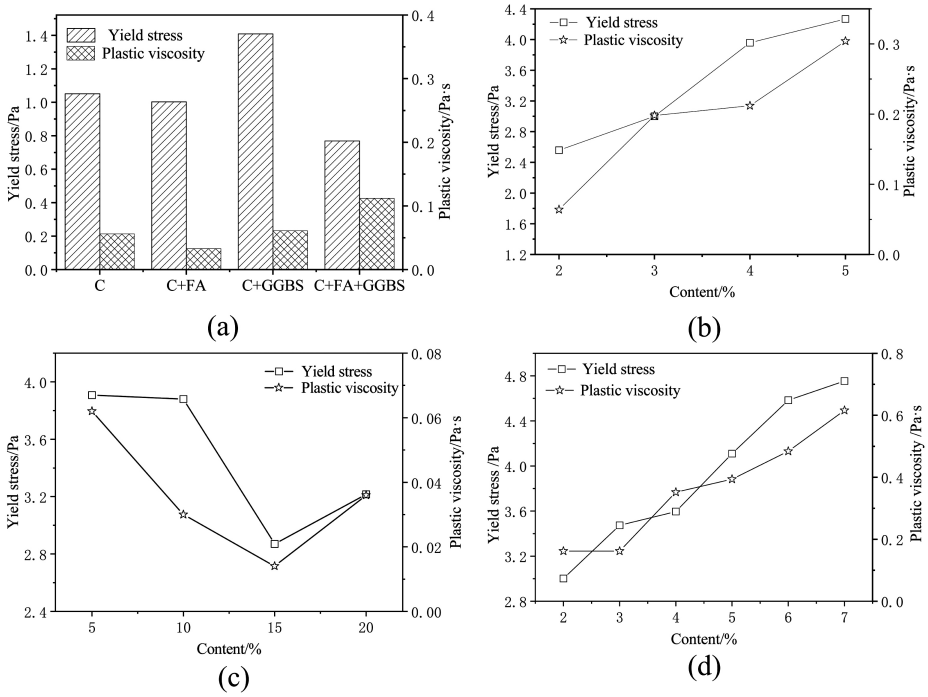

Fig. 7. Rheological properties of paste with different cementitious compositions
(a) FA, GGBS; (b) SF; (c) LP; (d) VMA

4.2. Stability of paste

The relationship between plastic viscosity and bleeding is shown in Fig. 8. There is a significant correlation between plastic viscosity and bleeding. Bleeding of paste descend evidently with the increasing plastic viscosity of paste. Bleeding of paste is zero when

plastic viscosity of paste exceeds 0.3 Pa·s. Hence, the threshold plastic viscosity of paste bleeding performance is obtained which can be used in paste design.

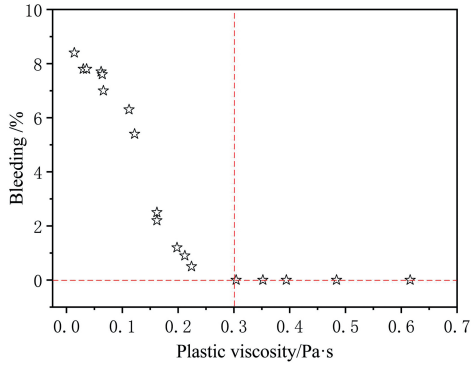

Fig. 8. Effects of plastic viscosity on bleeding

As illustrated in Fig. 9, plastic viscosity has remarkable effects on the surface bubble ratio θ of paste. In addition, the plastic viscosity has exponent relation to θ, the corresponding fitting formula is presented in Eq. (4.1). Surface bubble ratio $\theta$is less than 5% when plastic viscosity of paste is exceeding 0.394 Pa·s. Meanwhile, number of large bubbles is close to zero when plastic viscosity of paste is exceeding 0.225 Pa·s, as shown in Fig. 10. Based on the relationship between viscosity and bleeding and surface bubble rate of paste, the threshold of plastic viscosity is suggested to be 0.394 Pa·s.

$$\theta = 68.11 \times e^{\left(-\frac{\eta}{0.06}\right)} + 2.17 \qquad R^2 = 0.957 \tag{4.1}$$

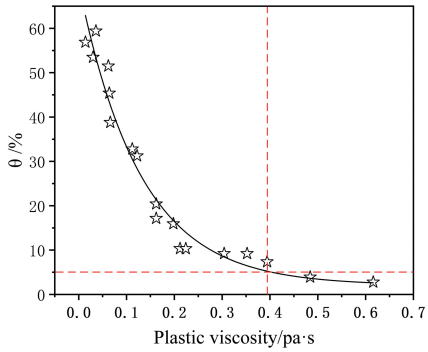

Fig. 9. Effects of plastic viscosity on θ

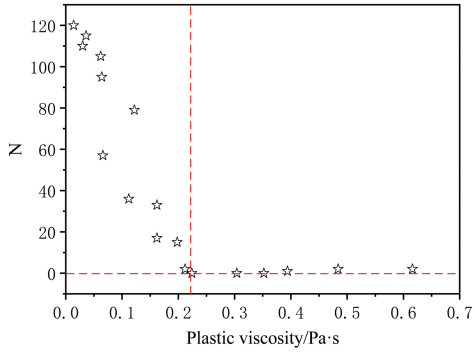

Fig. 10. Effects of plastic viscosity on N

Rheological property of paste was affected by water to binder ratio. The effect of water-binder ratio on paste viscosity was considered. The mixing proportions are listed in Table 4. Two series of paste were designed, the difference is the dosage of VMA and

water to binder ratio. Several contents of VMA (5%, 6%, 7%) or water to binder ratio by mass (0.32, 0.33, 0.34, 0.35, 0.36) were used. The results of plastic viscosity of paste with different VMA content and water to binder ratio are shown in Fig. 11. The corresponding fitting formula is provided in Eq. (4.2). According to the previous results that the threshold of plastic viscosity is 0.394 Pa·s, mix optimization in plastic viscosity aspect at paste level is performed. The area that satisfied the plastic viscosity criterion is shown in Fig. 12.

$$\eta_{\text{paste}} = 0.481 + 0.039 \times \alpha + 6.18 \times \left(\frac{W}{b}\right) + 0.023 \times \alpha^2 - 15.71 \times \left(\frac{W}{b}\right)^2 - 0.66 \times \left(\frac{W}{b}\right) \times \alpha \qquad R^2 = 0.98 \tag{4.2}$$

where: η is plastic viscosity, W/b is water to binder ratio, α is mass fraction of VMA.

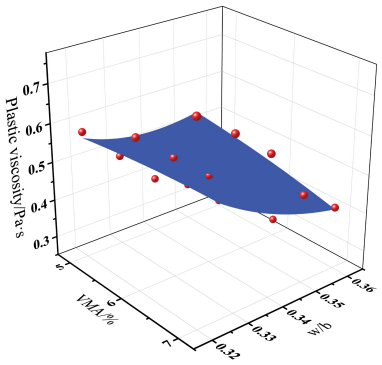

Fig. 11. Effects of VMA content and water-binder

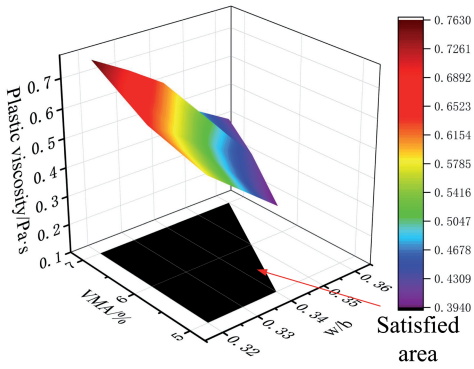

Fig. 12. Mixture satisfied area at paste level ratio on plastic viscosity

4.3. Stability of mortar

The results of measured slump flow of mortar with different η_{paste} and σ_{paste} are illustrated in Fig. 13. The relationship between slump flow, η_{paste} and σ_{paste} is shown in Eq. (4.3). According to experience, in order to ensure the good flow ability and filling ability of mortar, slump flow of mortar needs to be more than 280 mm. According to Eq. (4.3), threshold value of σ_{paste} is obtained when SCC does not occur segregation in flow process, these two criteria could ensure the mortar with high flow ability and ability to prevent aggregate segregation. The mix optimization of mortar is performed through above two criteria. The mixtures satisfied arear is shown in Fig. 14.

$$SF = 511.7 - 386.7e^{\left(-\frac{\sigma_{\text{paste}}}{0.29}\right)} \times e^{\left(-\frac{\eta_{\text{paste}}}{7.3}\right)} \qquad R^2 = 0.78 \tag{4.3}$$

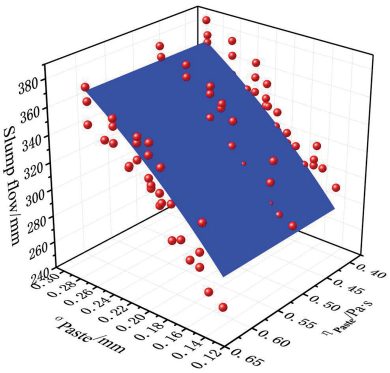

Fig. 13. Effects of σ_{paste} and η_{paste} on SF

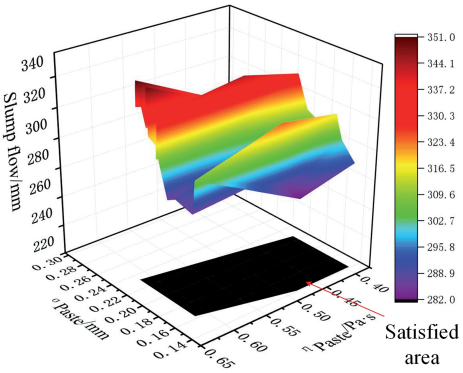

Fig. 14. Mixture satisfied area at mortar level

4.4. Stability of concrete

The workability of fresh SCC measured by slump flow, T500, passing ability, L with different λ_{ca} is shown in Fig. 15. It can be seen that slump flow and L values increase with λ_{ca} increasing. On the other hand, T500 and passing ability descend with λ_{ca} increasing. According to the requirement of China railway company standard [43] (Q/CR 596-2017),

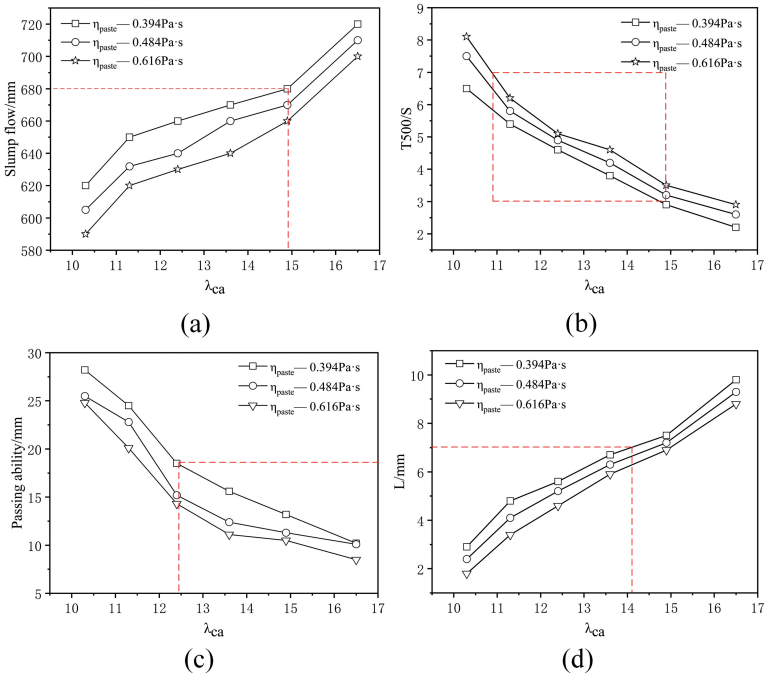

Fig. 15. Effects of λ_{ca} on workability of SCC; (a) slump flow; (b) T500; (c) passing ability; (d) L

the range of indices is $SF \leq 680$ mm, 3 s $< T500 <$ 7 s, J-Ring $<$ 18 mm $L <$ 7 mm [2,44], respectively. Mix proportion in λ_{ca} at concrete level is performed. 12.4 mm $< \lambda_{ca} <$ 14.1 mm is selected.

4.5. Verification the properties of scc for filling layer

Based on the research results of SCC stability from paste mortar and concrete, two mixing proportions (Mix No. 0.484-0.195-13.6 and 0.616-0.197-12.4, as listed in Table 5) are selected to verification stability of SCC through full-scale field experiment SCC filling layer construction. The filling layer of CRTS III ballastless slab track is constructed as the steps shown in Fig. 16. It can be seen that the construction procedures mainly include four steps. The first step is to place the bottom parts geotextile layer and reinforced mesh. Secondly, the prefabricated slab is put on the top of base plate. Then, the space between the base plate and slab is sealed, and the position of the slab is secured by clamps. Finally, SCC is cast into the sealed space from the pouring hole.

Fig. 16. The main construction steps of filling layer for CRTS III slab ballastless track; (a) Place geotextile layer and reinforced mesh; (b) Place prefabricated slab on the base plate at the presetting position; (c) Install formwork and clamps; (d) Cast concrete from the top pouring hole

After the completion of grouting SCC, the SCC filing layers are curing for 24 hours. Then prefabricated slabs are removed. Photographs of top surface of filling layer were taken, as shown in Fig. 17. From Fig. 17, defects such as laitance layer, water wave, foaming layer can't discovered on the top surface of filling layer. The area of one bubble is not more than 50 square millimeter which meets the requirements of Specification of self-compacting concrete for high-speed railway CRTS ? slab ballastless track [45]. The cross-section photographs of filling layer with two SCC mix proportions, as shown in Fig. 18. Segregation and settlement of SCC can't observe. Aggregates are distributed in

mortar uniformly and the thickness of top paste layer is thin. Through full-scale field experiment, we can see that the robustness SCC for filling layer is prepared and bleeding, segregation, surface settlement and instability of air bubble can be eliminated with the research results.

（a） （b）

Fig. 17. Photographs of top surface of filing layer; (a) Mix No. 0.484-0.195-13.6; (b) Mix No. 0.616-0.197-12.4

(a) (b)

Fig. 18. Photographs of cross-section of filing layer; (a) Mix No. 0.484-0.195-13.6; (b) Mix No. 0.616-0.19-12.4

5. Conclusions

- Evaluation indexes including bleeding B, surface bubble rate θ, thickness of paste σ_{paste} and thickness of surface paste L are proposed and the effectiveness of them are verified.
- When the plastic viscosity of paste is exceeding 0.394 Pa·s, bleeding of paste is eliminated and surface bubble rate of paste is bellowing 5%.
- Mix proportion satisfied area of paste is selected by theoretical research and experimental results.
- The workability of fresh SCC is influenced by λ_{ca} obviously. Finally, the optimum range of λ_{ca} is suggested to be 12.4~14.1 mm.
- The stability of SCC is verified by full-scale field experiment SCC filling layer construction. Defects such as laitance layer, water wave and foaming layer can't observe on the surface of filling layer. Stability of SCC for filling layer is improved by research results.

Acknowledgements

This work was supported by Doctor Launch Project of Liaoning province grant numbers 2021-BS-166 and Education Department Project of Liaoning province grant numbers lnqn202017

References

[1] Q. Yuan, G. Long, Z. Liu, et al., "Sealed-space-filling SCC: A special SCC applied in high-speed rail of China", *Construction and Building Materials*, 2016, vol. 124, no. 15, pp. 167–176, DOI: 10.1016/j.conbuildmat.2016.07.093.

[2] G. Long, H. Liu, K. Ma, et al., "Development of high performance self-compacting concrete applied for filling layer of high-speed railway", *Journal of Materials in Civil Engineering*, 2018, vol. 30, no. 2, art. ID. 04017268, DOI: 10.1061/(ASCE)MT.1943-5533.0002129.

[3] N. Li, L. Guang, F. Qiang, et al., "Dynamic mechanical characteristics of filling layer self-compacting concrete under impact loading", *Archives of Civil and Mechanical Engineering*, 2019, vol. 19, no. 3, pp. 851–861, DOI: 10.1016/j.acme.2019.03.007.

[4] X. Tao, D. Yu, et al., "Application of rubber mats in transition zone between two different slab tracks in high-speed railway – sciencedirect", *Construction and Building Materials*, 2020, vol. 243, art. ID. 118219, DOI: 10.1016/j.conbuildmat.2020.118219.

[5] X.W. Sheng, W.Q. Zheng, Z.H. Zhu, et al., "Full-scale fatigue test of unit-plate ballastless track laid on long-span cable-stayed bridge", *Construction and Building Materials*, 2020, vol. 247, art. ID. 118601, DOI: 10.1016/j.conbuildmat.2020.118601.

[6] V.K. Bui, et al., "Rapid testing method for segregation resistance of self-compacting concrete", *Cement and Concrete Research*, 2002, vol. 32, no. 9, pp. 1489–1496, DOI: 10.1016/S0008-8846(02)00811-6.

[7] L. Shen, H.B. Jovein, M. Li, "Measuring static stability and robustness of self-consolidating concrete using modified Segregation Probe", *Construction and Building Materials*, 2014, vol. 70, no. 15, pp. 210–216, DOI: 10.1016/j.conbuildmat.2014.07.112.

[8] P. Ghoddousi, A. Javid, J. Sobhani, "Effects of particle packing density on the stability and rheology of self-consolidating concrete containing mineral admixtures", *Construction and Building Materials*, 2014, vol. 53, no. 28, pp. 102–109, DOI: 10.1016/j.conbuildmat.2013.11.076.

[9] M. Sonebi, P. Bartos, "Filling ability and plastic settlement of self-compacting concrete", *Materials and Structures*, 2002, vol. 35, no. 8, pp. 462–469, DOI: 10.1007/BF02483133.

[10] M. Mouret, G. Escadeillas, A. Bascoul, "Metrological significance of the column test in the assessment of the static segregation of self-compacting concrete in the fresh state", *Materials and Structures*, 2008, vol. 41, no. 4, pp. 663–679, DOI: 10.1617/s11527-007-9272-7.

[11] J. Assaad, K.H Khayat, J. Daczko, "Evaluation of Static Stability of Self-Consolidating Concrete", *Aci Materials Journal*, 2004, vol. 101, no. 3, pp. 168–176.

[12] H.A. Mesbah, A. Yahia, K.H. Khayat, "Electrical conductivity method to assess static stability of self-consolidating concrete", *Cement and Concrete Research*, 2011, vol. 41, no. 5, pp. 451–458, DOI: 10.1016/j.cemconres.2011.01.004.

[13] B. Esmaeilkhanian, D. Feys, K.H. Khayat, et al., "New Test Method to Evaluate Dynamic Stability of Self-Consolidating Concrete", *Aci Materials Journal*, 2014, vol. 111, no. 3, pp. 299–307, DOI: 10.14359/51686573.

[14] L. Shen, H.B. Jovein, Z. Sun, et al., "Testing dynamic segregation of self-consolidating concrete", *Construction and Building Materials*, 2015, vol. 75, pp. 465–471, DOI: 10.1016/j.conbuildmat.2014.11.010.

[15] N. Tregger, A. Gregori, L. Ferrara, et al., "Correlating dynamic segregation of self-consolidating concrete to the slump-flow test", *Construction and Building Materials*, 2012, vol. 28, no. 1, pp. 499–505, DOI: 10.1016/j.conbuildmat.2011.08.052.

[16] *ASTM C1611 Standard test method for slump flow of self-compacting concrete (appendix)*. 2009.

[17] The self-compacting concrete European project group, *The European guidelines for self-compacting concrete: Production and Use*. EFNARC, 2005.

[18] B. Esmaeilkhanian, K.H. Khayat, A. Yahia, et al., "Effects of mix design parameters and rheological properties on dynamic stability of self-consolidating concrete", *Cement and Concrete Composites*, 2014, vol. 54, pp. 21–28, DOI: 10.1016/j.cemconcomp.2014.03.001.

[19] L. Shen, L. Struble, D. Lange, "Modeling Static Segregation of Self-Consolidating Concrete", *Aci Materials Journal*, 2009, vol. 106, no. 4, pp. 367–374.

[20] B.O. Koura, M. Hosseinpoor, A. Yahia, "Coupled effect of fine mortar and granular skeleton characteristics on dynamic stability of self-consolidating concrete as a diphasic material", *Construction and Building Materials*, 2020, vol. 263, art. ID. 120131, DOI: 10.1016/j.conbuildmat.2020.120131.

[21] N.A. Libre, R. Khoshnazar, M. Shekarchi, "Relationship between fluidity and stability of self-consolidating mortar incorporating chemical and mineral admixtures", *Construction and Building Materials*, 2010, vol. 24, no. 7, pp. 1262–1271, DOI: 10.1016/j.conbuildmat.2009.12.009.

[22] H.E. Chabib, M. Nehdi, "Effect of mixture design parameters on segregation of self-consolidating concrete", *ACI Material Journal*, 2006, vol. 103, no. 5, pp. 374–383.

[23] M. Mahdikhani, A.A. Ramezanianpour, "New methods development for evaluation rheological properties of self-consolidating mortars", *Construction and Building Materials*, 2015, vol. 75, pp. 136–143, DOI: 10.1016/j.conbuildmat.2014.09.094.

[24] K. Amini, I. Mehdipour, S.D. Hwang, et al., "Effect of binder composition on time-dependent stability and robustness characteristics of self-consolidating mortar subjected to prolonged agitation", *Construction and Building Materials*, 2016, vol. 112, pp. 654–665, DOI: 10.1016/j.conbuildmat.2016.02.226.

[25] P. Ghoddousi, A. Javid, J. Sobhani, "Effects of particle packing density on the stability and rheology of self-consolidating concrete containing mineral admixtures", *Construction and Building Materials,* 2014, vol. 53, no. 28, pp. 102–109, DOI: 10.1016/j.conbuildmat.2013.11.076.

[26] L. Shen, H.B. Jovein, Q. Wang, "Correlating aggregate properties and concrete rheology to dynamic segregation of self-consolidating concrete", *Journal of Materials in Civil Engineering*, 2015, vol. 28, no. 1, DOI: 10.1061/(ASCE)MT.1943-5533.0001325.

[27] L. Shen, L. Struble, D. Lange, "Modeling static segregation of self-consolidating concrete", *ACI Material Journal*, 2009, vol. 106, no. 4, pp. 367–374.

[28] F. Li, J. Wei, J. Wang, et al., "New Method of Mix Design for Self-Compacting Concrete Based on Material Characteristics", *Procedia Engineering*, 2012, vol. 27, no. 2, pp. 214–222, DOI: 10.1016/j.proeng.2011.12.446.

[29] S.E. Chidiac, F. Mahmoodzadeh, "Plastic viscosity of fresh concrete – A critical review of predictions methods", *Cement and Concrete Composites*, 2009, vol. 31, no. 8, pp. 535–544, DOI: 10.1016/j.cemconcomp.2009.02.004.

[30] N. Toutou, et al., "Multi Scale Experimental Study of Concrete Rheology: From Water Scale to Gravel Scale", *Materials and Structures*, 2006, vol. 39, no. 2, pp. 189-199, DOI: 10.1617/s11527-005-9047-y.

[31] A. Kwan, V. Wong, W. Fung, "A 3-parameter packing density model for angular rock aggregate particles", *Powder Technology*, 2015, vol. 274, pp. 154–162, DOI: 10.1016/j.powtec.2014.12.054.

[32] V.K. Bui, Y. Akkaya, S.P. Shah, "Rheological Model for Self-Consolidating Concrete", *ACI Materials Journal*, 2002, vol. 99, no. 6, pp. 549–559.

[33] I.N. Ariyanto, H.H. Purba, A. Purba, "A systematic review and analysis of risk assessment in highway construction project", *Operational Research in Engineering Sciences: Theory and Applications*, 2020, vol. 3, no. 3, pp. 29–47, DOI: 10.31181/oresta20303029a.

[34] E. Softić, V. Radičević, M. Subotić, et al., "Sustainability of the optimum pavement model of reclaimed asphalt from a used pavement structure", *Sustainability*, 2020, vol. 12, no. 5, art. ID. 1912, DOI: 10.3390/su12051912.

[35] B. Matić, S. Jovanović, M. Marinković, et al., "A Novel Integrated Interval Rough MCDM Model for Ranking and Selection of Asphalt Production Plants", *Mathematics*, 2021, vol. 9, no. 3, art. ID. 269, DOI: 10.3390/math9030269.

[36] H. Chen, W. Sun, Y. Zhou, et al., "Analytical solution of the nearest surface spacing between neighboring aggregate grains in cementitious composites", *Journal of the Chinese Ceramic Society*, 2005, vol. 33, no. 7, pp. 859–863, 870.

[37] H.S. Chen, W. Sun, P. Stroeven, et al., "Stereological method of calculating the average value of surface spacing between the neighboring aggregate grains in concrete", *Journal of Harbin Institute of Technology*, 2005, vol. 11, pp. 1511–1514.

[38] F.J. Rubio-Hernández, J.F. Velázquez-Navarro, L.M. Ordóñez-Belloc, "Rheology of concrete: a study case based upon the use of the concrete equivalent mortar", *Material and Structures*, 2013, vol. 46, no. 4, pp. 587–605, DOI: 10.1617/s11527-012-9915-1.

[39] T.K. Erdem, K.H. Khayat, A. Yahia, "Correlating Rheology of Self-Consolidating Concrete to Corresponding Concrete-Equivalent Mortar", *Aci Material Journal*, 2009, vol. 106, no. 2, pp. 154–160.

[40] K. Ma, J. Feng, G. Long, et al., "Influence of Rheological Parameters on Static Stability of Self-Compacting Concrete Equivalent Mortar", *Journal of the Chinese Ceramic Society*, 2017, vol. 45, no. 2, pp. 196–205, DOI: 10.14062/j.issn.0454-5648.2017.02.04 (in Chinese).

[41] *JTG3420-2020 Testing methods of cement and concrete for highway engineering*. Chinese National Standard, 2020.

[42] *ASTM C1611 Standard test method for slump flow of self-consolidating concrete*. ASTM International, 2009.

[43] *ASTM C1621 Standard test method for passing ability of self-consolidating concrete by J-ring*. ASTM International, 2009.

[44] G.C. Long, "Measurement of the stability of sealed-space-filling self-compacting concrete", Chinese Patent, No. CN201510236203.5, 2015.

[45] China Railway Company, *Q/CR 596-2017 Specification of self-compacting concrete for high-speed railway CRTS ? slab ballastless track*. China Railway Press, 2017.

Received: 13.02.2022, Revised: 12.04.2022